Seasonal snow cover on frozen ground: Energy balance calculations of a permafrost site near Ny-Ålesund, Spitsbergen

Julia Boike[1]
Alfred Wegener Institute for Polar and Marine Research, Potsdam, Germany

Kurt Roth and Olaf Ippisch
Institute of Environmental Physics, University of Heidelberg, Heidelberg, Germany

Received 11 June 2001; revised 3 May 2002; accepted 13 June 2002; published 10 January 2003.

[1] We apply an energy balance model to the snow cover for snowpack accumulation and ablation at a continuous permafrost site on Spitsbergen for the snow-covered periods from fall 1998 to winter 2000. The model includes net radiative, turbulent, ground, snow, and rain heat flux. The balance yields two distinct types of snow ablation: winter and spring ablation. Energy transferred by sensible heat and rain input reduces the snow cover during the winter, creating internal ice lenses and basal ice. The snowpack ablates during spring in two stages in both years. During the first stage, surface melt and subsequent internal freezing compact and reduce the snow cover, but no runoff is produced. This phase lasts more than twice as long as the second stage. During the second stage, which takes 14 days in both years, melt rates from the snowpack are represented well using the energy balance model. Ground heat fluxes are comparable during spring in both years, but the long persistence of the snow cover in 2000 delays the thawing of the ground. Due to the duration of the snow cover during spring snow melt of both years, the total energy supplied to the ground is significant, between 30 and 50% of the total energy supplied by net radiation. *INDEX TERMS:* 1823 Hydrology: Frozen ground; 1863 Hydrology: Snow and ice (1827); 1878 Hydrology: Water/energy interactions; 3307 Meteorology and Atmospheric Dynamics: Boundary layer processes; *KEYWORDS:* snow cover, snow melt, frozen ground, energy balance, Spitsbergen

Citation: Boike, J., K. Roth, and O. Ippisch, Seasonal snow cover on frozen ground: Energy balance calculations of a permafrost site near Ny-Ålesund, Spitsbergen, *J. Geophys. Res.*, *108*(D2), 8163, doi:10.1029/2001JD000939, 2003.

1. Introduction

[2] The formation (accumulation) and melting of a snowpack is an important feature in Arctic landscapes. The snow cover exercises considerable influence on the surface energy balance, since variations in snow cover change the surface albedo. Long-term measurements at Ny-Ålesund, Spitsbergen, show that the albedo remains above 80% until late May. After that, a rapid decrease in albedo occurs and snow usually disappears within two to four weeks [*Winther et al.*, 1999].

[3] According to *Dingman* [1994], the snow melt can be divided into a warming, ripening and output phase. During the first phase, the temperature of the snowpack is raised to isothermal conditions at the melting point. Additional energy input creates surface melt; water is retained in the snow up to the point where the liquid holding capacity is exceeded (ripening phase). This initiates the output phase, in which water flows out of the snowpack and the energy input is proportional to the produced meltwater. Most snow melt models with varying degrees of complexity are written to predict runoff during the last phase. The simplest model for the calculation of snow melt runoff is the temperature index model, in which a simple linear relation is obtained between air temperature and snow melt intensity. Many field studies have been undertaken in the Arctic to investigate snow melt processes on point or watershed scales using surface energy balance models [*Woo et al.*, 1983; *Young et al.*, 1997]. Some surface energy balance models neglect the snow and ground heat flux [*Harstveit*, 1984], while other models estimate the snow and soil heat content [e.g., *Kane et al.*, 1997; *Zhang et al.*, 1997]. Internal snowpack processes, such as meltwater percolating and refreezing and snow settling are included in numerical models such as CROCUS [*Brun et al.*, 1989] and SNTHERM [*Jordan*, 1991].

[4] The snow cover's physical properties, thickness, establishment and duration control the ground thermal regime. *Roth and Boike* [2001] found that a thicker layer of snow greatly reduced the heat exchange of the permafrost soil with the atmosphere. Soil cooling was about twice as pronounced during the winter of 2000 where the snow cover was about half as thick (about 0.4 m). *Zhang et al.* [1996]

[1]Now at Water and Environmental Research Center, University of Alaska, Fairbanks, Alaska, USA.

0148-0227/03/2001JD000939$09.00

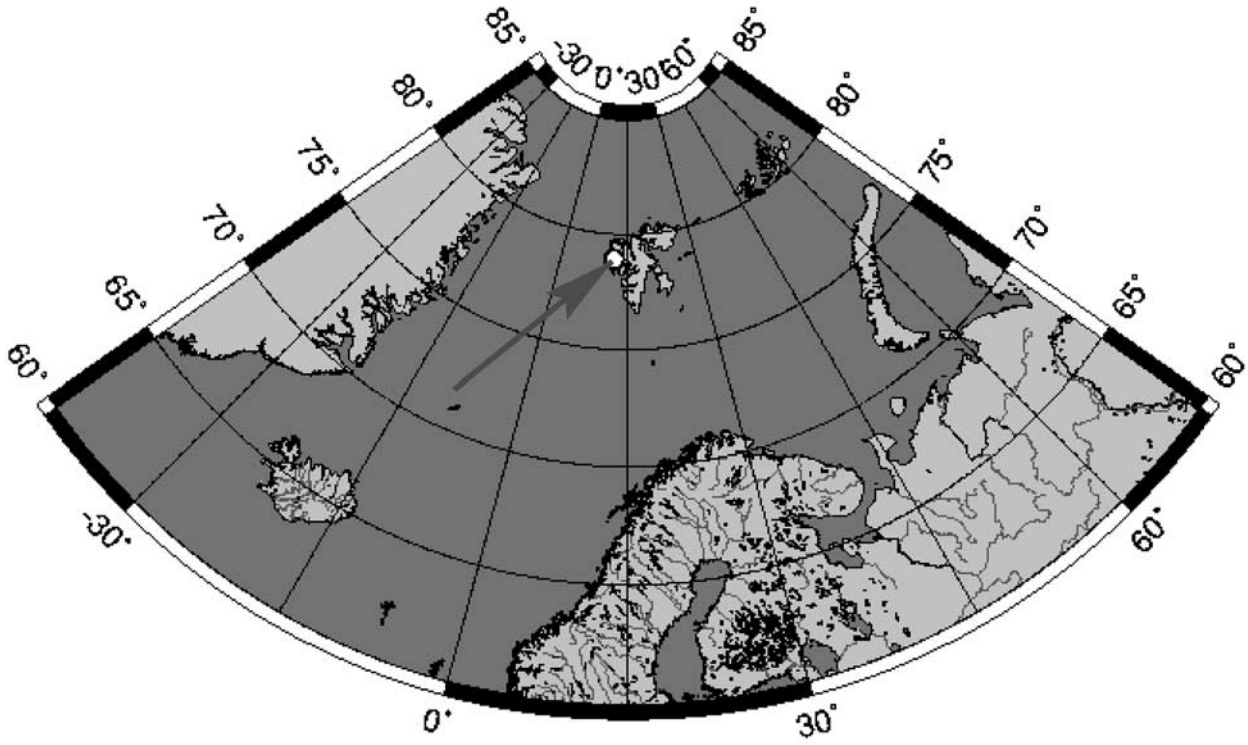

Figure 1. Geographical map showing the location of the study site in the high Arctic. The arrow indicates the area of the study site on west Spitsbergen.

showed that an increase of depth hoar, typically present at the base of the snowpack, can significantly increase ground temperatures and delay freeze back. *Sturm et al.* [2001] found recently that winter soil temperatures are substantially higher in Arctic shrubs where the snow cover is thicker due to trapping of snow. These areas also produced the highest CO_2 winter fluxes.

[5] The winter snow cover on Spitsbergen is unique for a high Arctic site since it contains internal ice lenses and basal ice. Our goal is to explore processes that govern the winter formation and ablation of the snow cover for the entire snow covered periods during the years 1999 and 2000. The melting of the snow cover and possible infiltration of snow meltwater and/or temperature induced vapor flux towards colder layers warmed the permafrost soil at this site down to depths of 0.9 m [*Roth and Boike*, 2001]. Thus our energy balance includes the ground heat flux. Energy balance components are quantitatively examined during the snow-covered period using highly resolved atmospheric and soil temperature and moisture data.

2. Site Description and Measured Data

[6] The Bayelva catchment is located about 3 km west from Ny-Ålesund, Spitsbergen at (78°55′N 11°50′E; Figure 1). Continuous permafrost in this region underlies coastal areas to depths of about 100 m and mountainous areas to depths greater than 500 m [*Liestøl*, 1977]. The North Atlantic Current warms this area to average air temperatures around 5 and −13°C in July and January, respectively, and provides about 400 mm annual precipitation falling mostly as snow between September and May [*Førland et al.*, 1997].

[7] Our study site is located some 30 m above mean sea level, on top of a small hill covered with unsorted circles. The bare soil circle centers range about 1 m in diameter and are surrounded by vegetated borders consisting of a mixture of low vascular plants, mosses and lichens. We instrumented one of these circles in August 1998 to automatically monitor hourly temperature and liquid water content [*Roth and Boike*, 2001]. A weather station measures hourly solar radiation, net radiation, air temperature, humidity, snow depth and rainfall within 5 m of the instrumented soil site. Net radiation, Q_n, was first measured using a Campbell Scientific Q 7 net radiometer, which was exchanged on 18 April 2000 (day 839) for an NR Lite net radiometer. All data are checked against the radiation balance measurements of the Koldewey research station, where instruments are maintained daily. Their field accuracy ranges between 10% (Q 7) and 20% (NR Lite). Further hourly data used from the Koldewey and Norsk Polar weather station include: atmospheric pressure, relative humidity (for days 257–839), wind speed (for days 686 to 839), rainfall (for days 257 to 578). Hourly rainfall data obtained from the Norwegian Meteorological Institute's automatic precipitation gauge were cross-checked with daily precipitation measurements collected from a manual gauge.

[8] Snow water content is measured using a vertically installed time domain reflectometry (TDR) probe. When the snow cover is less than the length of the snow TDR probe, l_0, the measured dielectric constant ϵ_m is corrected for the

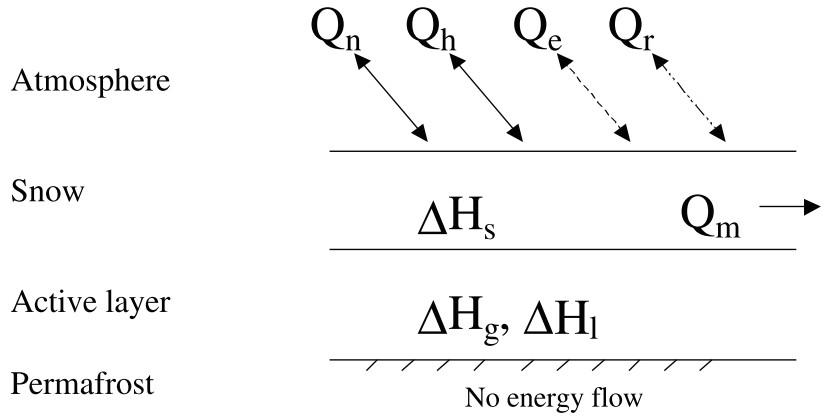

$$Q_n+Q_h+Q_e+Q_r = \Delta H_s+\Delta H_g+\Delta H_l+Q_m$$

Atmospheric fluxes are defined positive towards surface

'Storage' terms are defined positive when storage is increased

Figure 2. Schematic diagram of the volume energy balance model.

length of the probe exposed to air, l_a, to calculate the snow dielectric constant ϵ_s:

$$\epsilon_s = \left(\frac{l_0\sqrt{\epsilon_m} - l_a}{l_s}\right)^2, \quad (1)$$

where l_s is the snow depth. The length of the TDR probe is 0.5 m.

[9] The snow liquid water content θ_s is calculated following *Lundberg* [1997], applying an average snow density of 350 kg m^{-3}. Changing the snow density by 100 kg m^{-3} results in a absolute change in snow liquid water content of about 1%. Two temperature sensors are installed above the ground at 0.35 and 0.48 m height to record snow temperatures; between days 851 and 1035 the sensor at 0.35 m malfunctioned and after day 751 the sensor at 0.48 m failed completely. For these days, the air temperature is used as an approximation for snow temperature. Computed ground and snow heat flux data are smoothed using a cubic spline to eliminate high frequency changes in amplitude. Other snow physical characteristics (density, temperature, stratigraphy) were measured in snow pits during May and June of 1999 and 2000 (K. Sand, unpublished data, 2001) and on 20 April 2000 using standard methods.

[10] Hourly data collection started in September 1998. The data spans more than two years, from 14 September 1998 to 24 January 2001 (day 1120).

3. Model Description

[11] A simple volume energy balance of a snowpack may be formulated as:

$$Q_n + Q_h + Q_e + Q_r = \triangle H_g + \triangle H_l + \triangle H_s + Q_m\ , \quad (2)$$

where Q_n is the net radiation balance, Q_h and Q_e are turbulent fluxes of sensible and latent heat and Q_r is the heat flux supplied by rain (Figure 2). The terms on the right side of the equation describe the soil and snow's change in thermal energy. The rate of heat flow into soil and snow is calculated as change of the sensible and latent heat per unit time (hourly time steps).

[12] The thermal energy stored as sensible heat at time t in soil to a depth of 1.13 m, $H_g(t)$, and in the snowpack, $H_s(t)$, is estimated by the summation over the phases ice i and fluid w and soil matrix sm along the vertical axis of soil and snow z [*Boike et al.*, 1998]:

$$H_{g,s} = \sum_{\alpha\in i,w,sm} c_\alpha \rho_\alpha \int \theta_\alpha(z,t)T(z,t)dz\ , \quad (3)$$

where c_α is specific heat capacity, ρ_α mass density, θ_α volumetric content of phase α and T temperature. For calculation of snow heat content, the ice thermal capacity and density are set to $C_s = 2.11 \cdot 10^3$ J kg^{-1} K^{-1} and 350 kg m^{-3}, respectively.

[13] The term H_l is the latent heat of ground and is calculated as:

$$H_l = -L_f \rho_i \int \theta_i(z_g,t)dz\ , \quad (4)$$

where θ_i is the ice content estimated from TDR measurements of unfrozen water content and from soil water content before freeze-back. This implicitly assumes that no significant moisture redistribution takes place during winter. $L_f = 0.333 \cdot 10^6$ J kg^{-1} is the latent heat of fusion. Since our instruments extend below the depth of seasonally thawing and freezing ground, ground heat fluxes below 1.13 m are negligible within the context of this paper. The reference state for the energy storage calculations is liquid water at 0°C. The latent heat flux of the snowpack, Q_m, is the remainder in the balance. For $Q_m > 0$, melting is expected

while for $Q_m < 0$, freezing and recrystallization are expected. The estimated potential error in Q_m lies between ±15 and 25%.

[14] Atmospheric fluxes (defined here as Q_n, Q_h, Q_e and Q_r) towards the snowpack are defined as positive (energy gain), away from it as negative (energy loss). In contrast to simple surface energy balance equations applied for snow melt modeling at a point, this approach considers the changes of sensible and latent heat of ground and snow. Since the rain heat flux is generally small, this term is often ignored in snow melt studies [*Zhang et al.*, 1997], but we include it here since winter rain events are common at this site on Spitsbergen.

[15] Since accurate measurements of snow surface temperature, T_s at unsupervised, remote, Arctic sites are extremely difficult to obtain, they are often estimated using the air temperature T_a. Here T_s is estimated with the formula of *Woo et al.* [1999] using the average T_a of the past (t_{i-1}) and present (t_i) time step (hourly measurements):

$$T_s(t) = \frac{T_a(t_{i-1}) + T_a(t_i)}{2} \ , \tag{5}$$

for $T_a(t_i) < 0$. For $T_a(t_i) \geq 0$°C, $T_s = 0$°C.

[16] Turbulent heat fluxes Q_h and Q_e are governed by the complex exchange processes in the lower atmosphere. A common parameterization in snow melt models is the bulk aerodynamic formulae by *Price and Dunne* [1976]:

$$Q_h = \rho_a C_a D_{h(n,s,u)}(T_a - T_s) \ , \tag{6}$$

$$Q_e = \rho_a L_{(v,s)} D_{e(n,s,u)}(0.622/p)(e_a - e_s) \ , \tag{7}$$

where ρ_a and C_a are the density and specific heat of air, D_h and D_e are heat and vapor transfer coefficients for neutral (n), stable (s), unstable (u) conditions, T_a is the temperature at 2 m height, $L_{(v,s)}$ is the latent heat of vaporization or sublimation ($2.48 \cdot 10^6$ J kg^{-1} and $2.83 \cdot 10^6$ J kg^{-1}, respectively), p is atmospheric pressure, e_a is vapor pressure at 2 m height and e_s is ice saturated vapor pressure over a cold snowpack ($T_s < 0$°C) or water saturated vapor pressure over a melting snowpack ($T_s = 0$°C).

[17] The direction of Q_e and the surface temperature determine whether vapor condensates, sublimates or resublimates (phase change from vapor to ice). If Q_e is positive, i.e., directed towards the surface, and $T_s = 0$, the surface experiences condensation and L_v is applied; if $T_s < 0$°C, resublimation occurs and L_s is used. For negative heat fluxes, snow always sublimates independent of T_s and L_s is applied.

[18] The heat and vapor transfer coefficients D_h and D_e are assumed to equal that for momentum D_m. For neutral conditions they can be estimated as:

$$D_{h(n)} = D_{e(n)} = D_{m(n)} = \frac{u_{z_i} k^2}{(ln(z_i/z_0))^2} \ , \tag{8}$$

where k is the von Kármán constant (=0.41), u_{zi} is wind speed at instrument height z_i and z_0 is the roughness length, assumed to be constant at 0.16 mm over the measurement period.

[19] Following *Price and Dunne* [1976], the bulk Richardson number, R_i, is used to adjust for atmospheric conditions other than neutral:

$$R_i = \frac{g\Delta z_i(T_a - T_s)}{\left(u_{z_i}^2 T_a\right)} \ , \tag{9}$$

where the term Δz_i is the distance between instrument height and snow surface, T is absolute temperature (K) and g is the gravitational constant.

[20] If conditions are stable ($R_i > 0$), the stable transfer coefficient is:

$$D_{h(s)} = D_{h(n)}/(1 + 10R_i) \ , \tag{10}$$

and for unstable conditions:

$$D_{h(u)} = D_{h(n)}(1 - 10R_i) \ . \tag{11}$$

The bulk transfer equations and stability adjustment have successfully been applied in various settings in the Arctic [e.g., *Woo et al.*, 1999; *Hinzman et al.*, 1991; *Kane et al.*, 1997]. *Tarboton et al.* [1995] reported unreasonable correction factors during times of large temperature differences and low wind speeds and thus used neutral transfer coefficients only. At higher wind speeds, common at our site, a high temperature difference results only in small variations in the correction factor [*Braithwaite*, 1995].

[21] Assuming that the rain has the same temperature as the air, the heat flux supplied by rain is computed using rainfall rate and air temperature.

[22] The following assumptions were made for the snow melt computations: (1) When energy balance is positive, surplus energy is consumed by snow melt; (2) a snow cover with homogeneous density and thermal capacity is assumed at the onset of the snow melt computation; (3) heat transfer is assumed to be instantaneous.

[23] The rate of surface snow melt, M, is expressed as snow water equivalent (SWE) and is calculated from the energy balance equation as:

$$M = Q_m/\left(\rho_w L_f\right) \ , \tag{12}$$

where ρ_w is the density of water and from

$$M = \frac{\rho_s}{\rho_w}\frac{dz_s}{dt}, \tag{13}$$

where z_s is the thickness of the snowpack, t is time and ρ_s is the density of snow. Snow densities were measured daily in snow pits at a site nearby during premelt and melt period (K. Sand, unpublished data, 2001). Since density variations between sites are large, a range of snow densities is used for the calculation of surface melt in equation (13). The average vertical snow density between 19 May and 13 June 1999 ranged between 377 and 487 kg m^{-3} (average 455 kg m^{-3}) and from 9 May to 27 July 2000 between 350 and 478 kg m^{-3} (average 423 kg m^{-3}). Based on the average density field data, a snow density range between 350 and 500 kg m^{-3} is used for the calculation of surface melt from

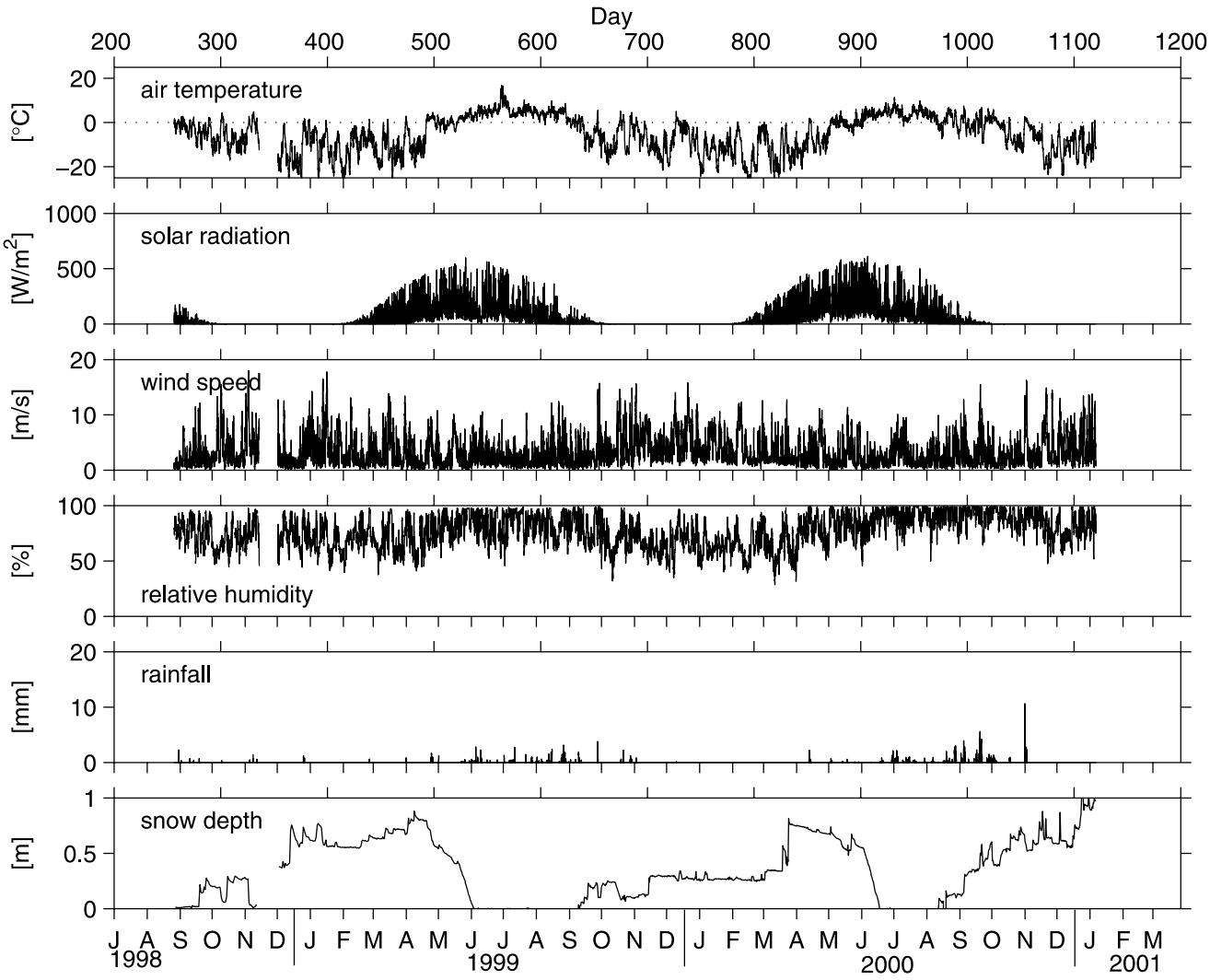

Figure 3. Measured meteorological variables (air temperature, solar radiation, wind speed, relative humidity, rainfall, snow depth).

equation (13). The calculated surface melt rates in equations (12) and (13) do not necessarily predict melt flowing out of the snowpack. As discussed earlier, the energy input and meltwater production are linearly related during the output phase only.

4. Results

4.1. Climate and Snow Cover

[24] The meteorological record from September 1998 to January 2001 is shown in Figure 3. Solar radiation turns positive around days 410 and 775 (14 February 1999 and 2000) and stays positive for about 260 days until about November 1st. Solar radiation input peaks during the snow melt season. Air temperatures typical of a mild, maritime winter show the influence of the Atlantic current in this high Arctic setting. Often, air temperatures above 0°C occur in combination with rainfall and higher wind speeds. Wind speed is highest during the winter periods, reaching averaged maximum values of 18 m s^{-1}. Relative humidity is lowest during the cold winter period, but reaches values between 90 and 100% during the snow melt period and during the summer. Rain falls regularly during the snow free periods. Furthermore, rain falls frequently on snow during the cold snow period (which interrupts the accumulation of snow) and during snow melt. Overall, the predominance of snow cover is obvious: From a total of 864 days, only 154 days are snow free. The snow cover is highly variable over time as a result of fresh snowfall, compaction and rain events. The first snow period lasts about 250 days and is shorter than the second snow period (about 290 days). Although the duration of the second snow period is longer, the thinner, 0.3 m snow cover persists longer compared to the first snow period. The third build up of snow starts around day 975 (2 September 2000) and its accumulation is very irregular. The greatest snow depth of more than 1 m is recorded on day 1108 (12 January 2001).

4.2. Energy Balance Components

[25] Throughout the winter Q_n remains negative when solar radiation input is zero (Figure 4). Even though solar radiation becomes positive in early spring, Q_n stays negative due to the high albedo of the snow cover. Following

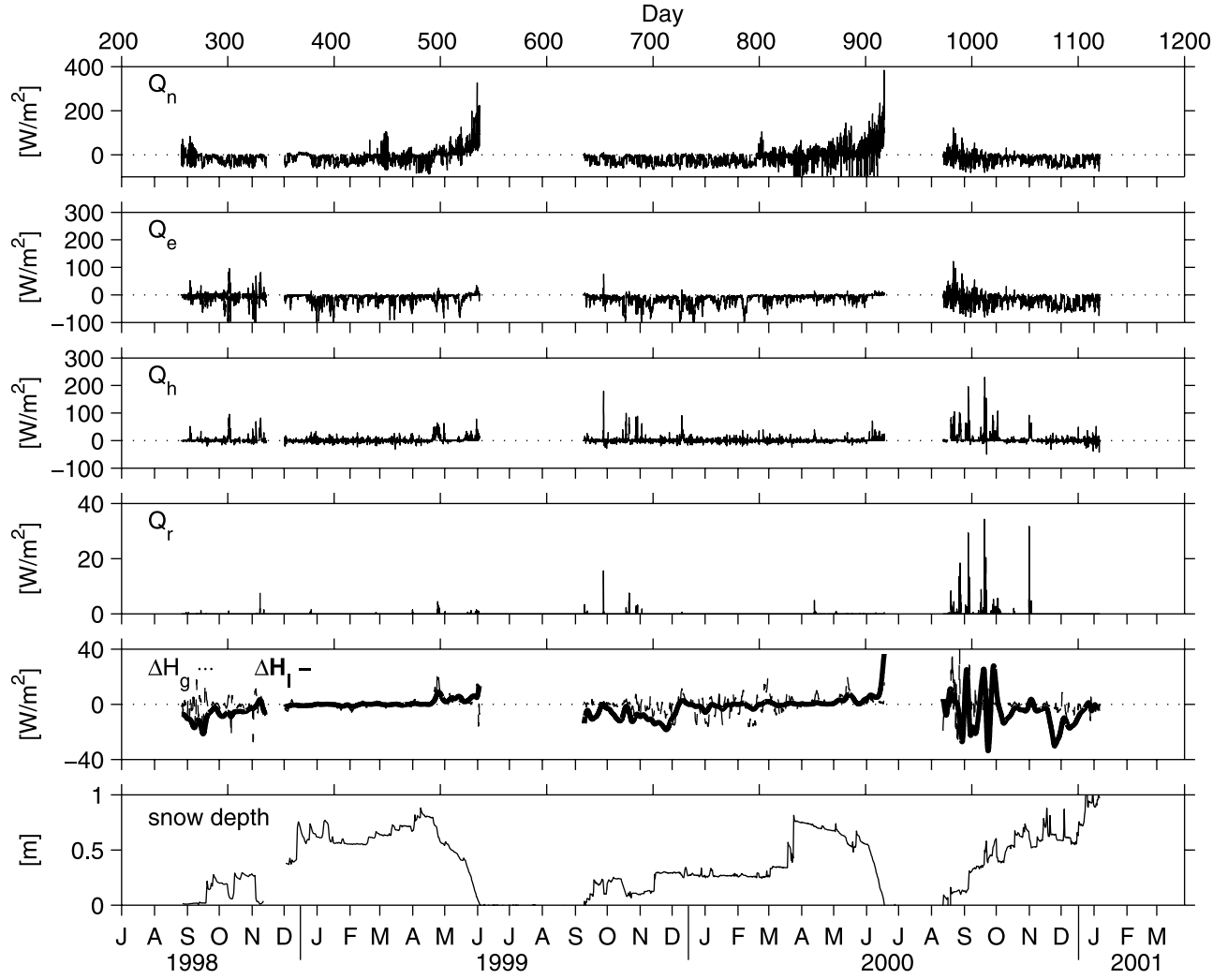

Figure 4. Measured net radiation (Q_n), estimated values of atmospheric sensible (Q_h) and latent (Q_e) and rain (Q_r) heat flux. The ground heat flux is partitioned into sensible (ΔH_g) and latent heat (ΔH_l) flux. Snow depth is shown again to visualize the snow covered periods from 1998 to 2000. No data are shown during snow free periods; data around day 350 are missing due to instrument failure.

ablation and change of snowpack physical properties during spring (day 490 and day 840), Q_n values increase towards positive values.

[26] Sensible heat fluxes, Q_h, away from the snow surface are generally small during the winter period. Positive Q_h fluxes are a significant heat input when the air temperature during the winter rises above 0°C. These events occur with rain events of low intensity throughout the snow-covered period. These rain events supply small amounts of Q_r, with maximum fluxes of about 35 W m^{-2}. Q_e fluxes are generally small and negative throughout the winter snow-covered period. Positive Q_e fluxes, such as those detected toward the end of the snow melt period, indicate condensation at the snow surface. This process is a potentially important energy source for melt, since the release of L_v is about 7.5 times larger than L_f. For this site, however, the contribution of Q_n and Q_h dominate the energy balance. Generally, Q_e fluxes compare well with those calculated during snow melt period by the aerodynamic profile method and bulk methods from snow models CROCUS and SNTHERM (A. Semadeni-Davies et al., manuscript in preparation, 2002).

[27] The heat flux of the ground (ΔH_g and ΔH_l) is a small term in the energy balance, ranging between ±40 W m^{-2}. More than half of the total ground heat flux is ΔH_l, thus an important energy term for the ground. During freeze back, ΔH_l is negative since energy is released from the ground into the snowpack due to the release of latent heat and vice versa, is consumed during spring warming. Total ground heat flux during freeze back is more negative during the second period (days 650–720) compared to the first snow-covered period (days 250–320) due to the thinner snow cover. The ground receives energy during the second snow-covered period (days 800–900; March to June 2000), while snow accumulates and with the start of positive net radiation. The latent heat of the refreezing snow cover is a possible source of energy, as is suggested by the drop in snow liquid water content (Figure 5). The larger fluctuations of ΔH_g during the onset of the third snow-covered period are connected to large energy inputs by Q_h, Q_e and Q_r,

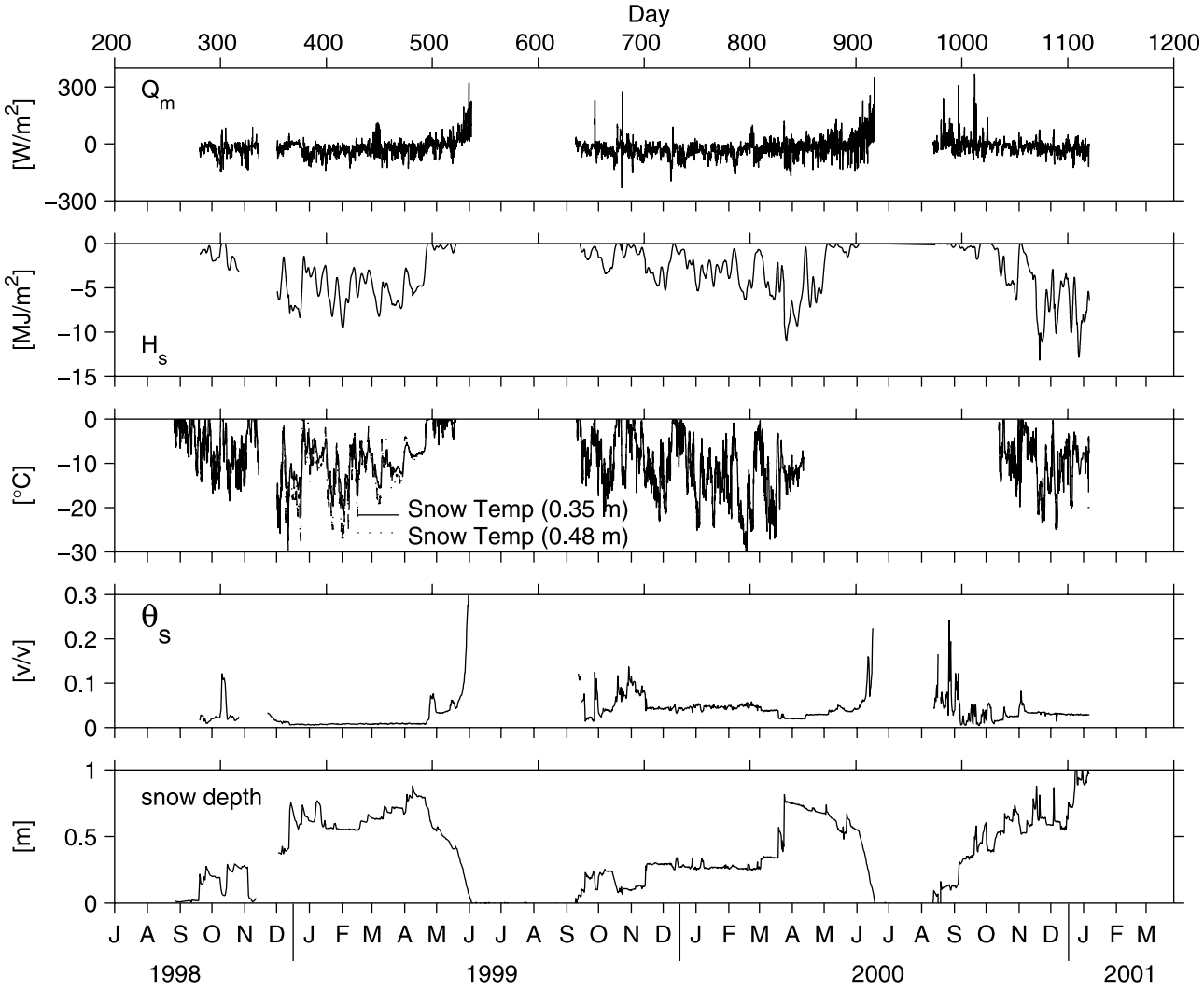

Figure 5. Melt energy Q_m, calculated from the energy balance equation (2), and snow physical properties: snow heat content (H_s), snow temperature, snow volumetric liquid water content (θ_s) and snow depth. The high snow liquid water content during the end of the 1999 snow melt (30%) is the result of slush snow and/or standing water conditions.

hence to repeated interruption of cooling and freezing of the ground.

4.3. Snow Internal Processes During Winter 1999/2000

[28] During the period of no solar radiation input, Q_m is supplied predominantly by Q_h and to a smaller extent by Q_r. In combination with a thinner snow cover, a positive Q_m causes a drastic decrease in snow cover (i.e., days 300, 330, 650, 680–700; Figure 5).

[29] Further insight into the relationship between snow cover physical characteristics and energy balance components may be gained from Figure 5. The snow sensible heat content, expressed in MJ m^{-2}, is quite variable due to fluctuations in temperature and snow thickness; with increasing snow depth or decreasing temperature, the negative heat content increases.

[30] Differences between positive melt events can be demonstrated by examining the Q_m events around days 301 (supplied by Q_h) and around 450 (supplied by Q_n). During the first event, sensible heat transfer is 95 W m^{-2}, yielding positive melt energy of about 70 W m^{-2}. In the second event, similar amounts of energy are supplied, ranging between 50 and 100 W m^{-2} over seven days. During the first event, the snow sensible heat content is high. Meltwater percolates through the snowpack (''through flow'') and infiltrates into the soil. This interpretation is supported by the measured increase of soil volumetric water content [*Roth and Boike*, 2001]. Refreezing of meltwater within or on top of the soil releases latent heat, warming the soil down to 0.5 m depth. Depending on the temperature regime and infiltration capacity of the ground, this process can create a basal ice layer.

[31] During the second event, energy is supplied to a cold, stratified snowpack. The snow is warmed rapidly (the probe at 0.48 cm height warms from about −17° to −5°C) and the temperature gradient reverses. The snow heat content increases, but it is still very low so that meltwater generated on the snow surface percolates and refreezes in the upper snowpack. The snow liquid water content does not show an increase in the lower 0.50 m of the snowpack,

suggesting a limited percolation and the creation of ice within the snowpack.

[32] Both of these snow stratigraphic characteristics, basal ice on the ground surface and snowpack ice structures, are identified in snow pits close to the site (Figure 6) and are characteristic for this area [*Gerland et al.*, 1999]. In both cases, percolating water and subsequent freezing act as an energy source.

[33] The snow temperature profile is further discussed using days 360 to 500 (December 1998 to May 1999), i.e., when probes are completely covered with snow. Snow temperature and air temperature differ by up to 20°C between days 460 and 500, a time when the snow cover depth increases to about 0.8 m. Freshly fallen snow effectively insulates the snowpack during this large air temperature change. The snow temperature at 0.35 m is dampened from the surface signal, and differs by up to 8°C from the air temperature.

4.4. Snow Melt in 1999 and 2000

[34] The start of surface snow melt computation in 1999 is determined as the point in time when snow depth begins a continuous decrease in spring. Air temperatures are below 0°C at the onset of snowpack ablation and remain close to 0°C during further progress of melt, probably stabilized by the snow cover. A warming event (supplied by Q_r and Q_h) in the beginning of May in 1999 (day 490), causes the snow temperature gradient to reverse (i.e., temperature at the upper probe became warmer than at the lower probe) and to become isothermal at 0°C. The snow liquid water content rises from 1 to 7.5% (Figure 5), i.e., meltwater percolates within the snowpack. As a result of the physical change of the snow (increase in effective snow grain size and hence decreased albedo), the optical properties of the snow cover change and Q_n increases. Cold air temperatures on the following days interrupt this process, and the meltwater refreezes again, as suggested by the drop in snow liquid water content. The observation that snow cover internal processes (involving percolating and refreezing meltwater) are responsible for reducing the snow height, but not the SWE, until day 523 (7 June 1999) is supported by: (1) the sensible heat content of snow turns zero after day 523 (Figure 5) (2) the snow liquid water content continuously increases after day 523 (Figure 5) (3) cumulative Q_m is negative up to day 523, i.e., refreezing is predicted (Q_m becomes positive on day 523; Figure 7a) (4) runoff is observed visually starting on day 523. Two stages of snowpack ablation can be defined (Figures 7b and 7c): when the snow heat content is still varying (diurnal variations), snow internal processes such as refreezing, physical changes (densification/settling) are at work. These processes result in a decreasing snow cover, not in SWE, and thus no runoff from the snowpack is produced. During the first stage of ablation, measured and modeled ablation rates do not agree since the cumulative sum of Q_m remains negative. When only positive Q_m values are used in the calculation (i.e., both the overnight refreezing of snow and internal processes are ignored), as in simple surface energy balance models, a closer fit between modeled and measured ablation data is obtained (Figure 7b). As discussed above, this does not reflect the physical processes of the snow cover. When the model is started on day 523, once the conditions for melt from the snowpack are met, the modeled and measured ablation rates agree reasonably well, assuming a snow density in the range of 350 kg m^{-3} to 500 kg m^{-3}. Slight changes in snow density and snowpack heterogeneity are expected to affect the SWE estimated from measured snow depths.

Figure 6. Snow pit dug close to the instrumented site in June 1998 showing internal ice lenses and basal ice. Snow was manually removed between the ice layers to underline the stratigraphy. Total snow depth was 0.55 m.

[35] The cumulative sum of energy balance components during snow ablation in 1999 is shown in Figure 7a. The dominant source of energy for melt is provided by Q_n (radiative melting). Q_h contributes about 30% of Q_n over the entire period, but 2/3 are generated during the first stage. Thus Q_h plays a minor role in the energy budget of the melt stage. Q_r and ΔH_s are the smallest terms and do not play an important role in the energy balance. Evaporation and sublimation use about 30% of Q_n, but since the latent heat involved is large, the ablation rate is low. This agrees with values from A. Semadeni-Davies et al. (manuscript in preparation, 2002), who found that 20 to 30% of Q_n was lost to evaporation during this period.

[36] The snow ablation calculations in 2000 are started on day 840 (19 April 2000). At this time, the snowpack is thermally stratified (−13.6°C on surface, −15.5°C at 0.10 m, decreasing to −9.6°C at 0.8 m depth), four major stratigraphic units are identified and densities range between 350 and 400 kg m^{-3}. Measured snow densities increase to

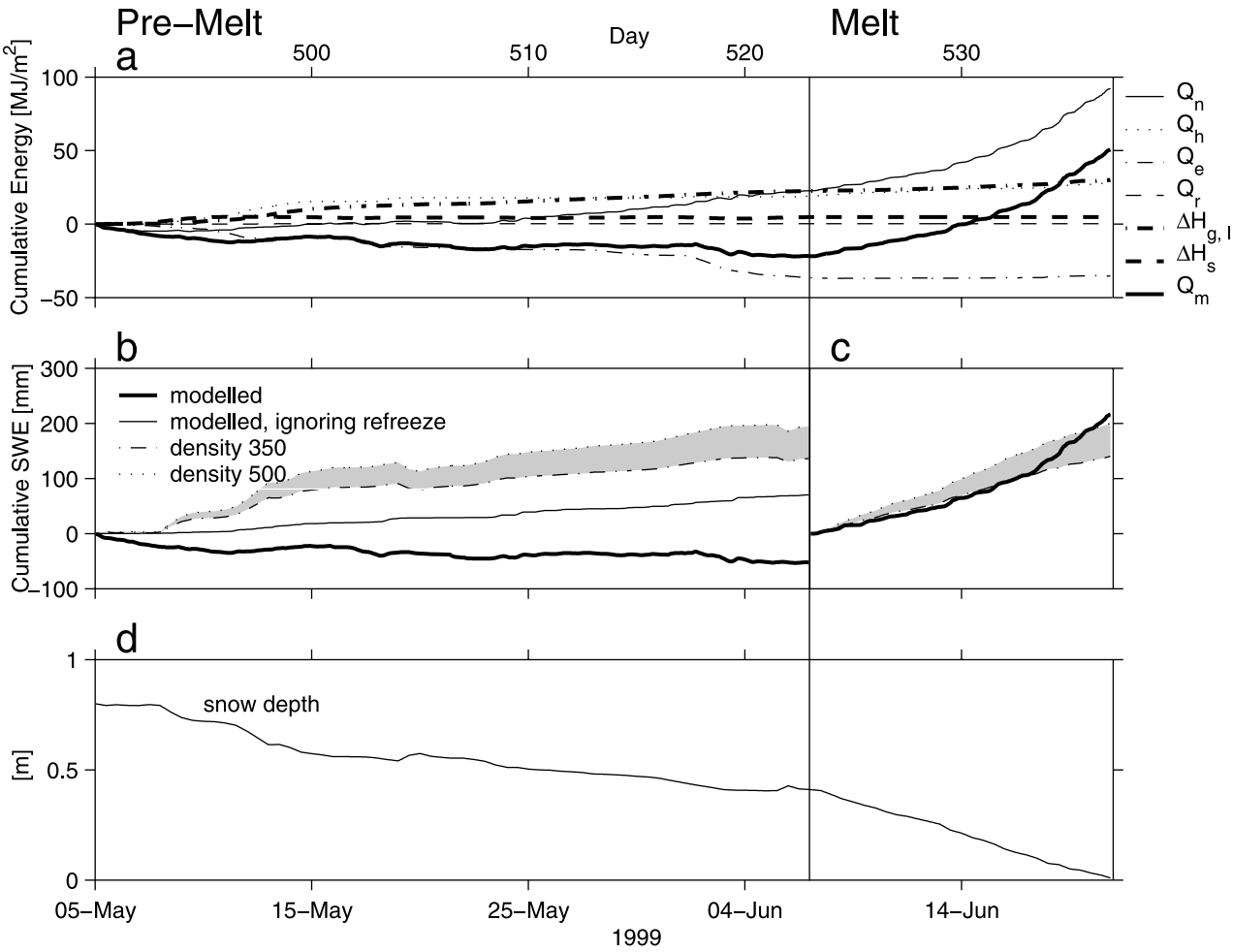

Figure 7. Cumulative energy balance components (a), melt rates expressed as cumulative snow water equivalents (b and c) and snow depth (d) for the premelt and melt period from 5 May to 21 June 1999 (days 504 to 537). Modeled melt rates, calculated using Q_m from the energy balance, are compared to melt rates obtained from snow depth measurements and a range (gray zone) of snow densities between 350 and 500 kg m^{-3}. Modeled ablation rates ignoring refreeze are calculated using positive Q_m values only.

an average value of about 445 kg m^{-3} toward the end of snow melt. Snow ablation in 2000 resembles that of 1999 in that two significant stages (premelt and melt) can be identified (Figures 8b and 8c). During the first stage, the cumulative sum of Q_m remains negative and snow internal processes compact the snow cover. Output of melt starts on day 903, again supported by field measurements of the snow liquid water content, which show a rapid and continuous increase after this day. As in 1999, Q_n increases concomitant with an increase of snow liquid water content; after fresh snow fall on day 890 (8 June 2000), Q_n drops. The model is started when Q_m values become and remain positive and a excellent fit of measured and modeled ablation rates is obtained (Figure 8c). Similar to 1999, ablation is driven by Q_n, Q_h increases during the second stage of ablation and Q_r and ΔH_s are the smallest terms.

4.5. Difference Between Snow Melt Processes of the Two Years

[37] A comparison of snow melt processes and energy balance components shows distinct differences between the two years. The ablation of snow starts later in 1999 (5 May) compared to 2000 (19 April) and takes half of the time to melt, about 47 days in 1999 and 78 days in 2000. The rate of snow melt during the second stage of ablation is higher in 2000, about 0.036 m/d compared to 0.028 m/d in 1999, with comparable melt energy inputs (using snow depth data). During both years ablation is initiated by Q_n, which remains the dominant energy source. The snow cover persists for a long time during the premelt stage of warming and ripening, 33 days in 1999 and 63 days in 2000, respectively. This is followed by a short melt stage (14 days in both years), in which meltwater is produced from the pack.

4.6. Snow Cover and Ground Heat Flux

[38] The thicker snow cover during the first winter reduces the heat exchange with the atmosphere [*Roth and Boike*, 2001]. Thus the ground heat content immediately before snow melt in 1999 (day 490) is −82 MJ m^{-2} whereas a thinner snow cover during the second winter results in a ground heat content just before snow melt (day 840) of −113 MJ m^{-2}.

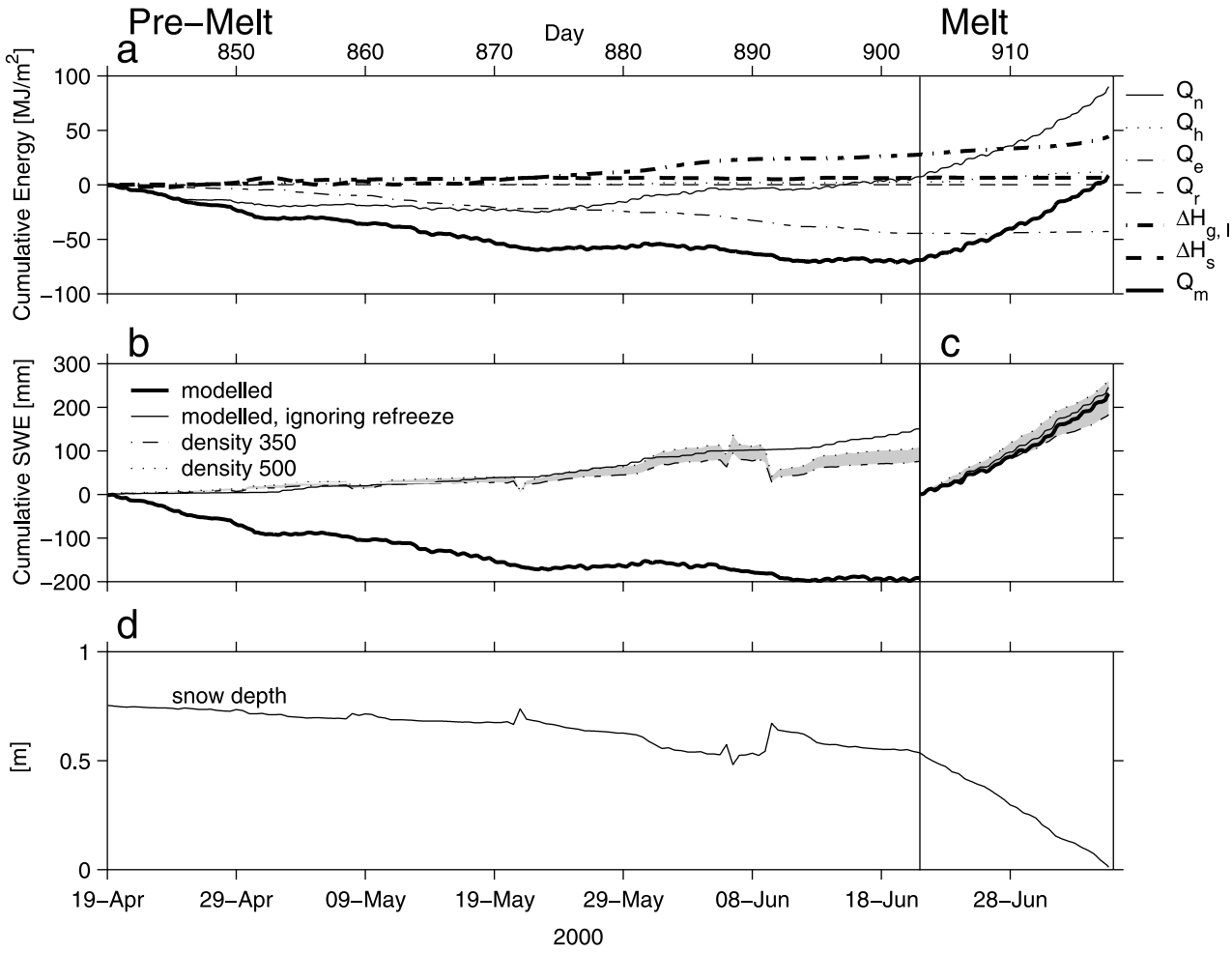

Figure 8. Cumulative energy balance components (a), melt rates expressed as cumulative snow water equivalents (b and c) and snow depth (d) for the premelt and melt period from 19 May to 6 July 2000 (days 870 to 918). Modeled melt rates, calculated using Q_m from the energy balance, are compared to melt rates obtained from snow depth measurements and a range (gray zone) of snow densities between 350 and 500 kg m^{-3}. Modeled ablation rates ignoring refreeze are calculated using positive Q_m values only.

[39] Due to the prolonged snow melt period in 2000, the total heat supplied to the ground is larger in 2000 than in 1999. The total amount of energy supplied to the ground during snow melt in 2000 (days 840 to 917) is about 44 MJ m^{-2} and in 1999 (days 490 to 537) 30 MJ m^{-2}. The average heat fluxes supplied during ablation are quite similar, about 6.3 W m^{-2} in 2000 and 7.5 W m^{-2} in 1999. During both years, the heat supplied to the ground during snow melt is a significant energy sink, using up to 50% of the total energy supplied by Q_n.

5. Conclusion

[40] The maritime climate of this high Arctic permafrost site makes it unique. Warm weather events during the winter interrupt the build up of the snow cover. Depending on the heat content of the snowpack, either internal ice lenses or basal ice are created. At other high Arctic settings (e.g., Canadian high Arctic), internal ice and basal ice layers are usually formed during spring melt [*Marsh and Woo*, 1984], and are thus not a biological barrier during the winter.

[41] Depending on the snow's physical properties, winter thaw events warm the soil through convective heat transfer, a process ignored when the soil thermal regime is modeled using conduction only. This supports the observation by *Putkonen* [1997], who found warming of the soil as a result of winter rain events in 1985/86. Furthermore, a snow cover of longer duration or increased thickness has a warming impact on the ground thermal regime, as the comparison between 1999 and 2000 shows. On the other hand, the long duration of the spring melt period results in a significant loss of heat to the ground.

[42] The energy balance model depicts two distinctly different stages of spring melt. During the first stage, surface melt infiltrates the snow which has a negative heat content. The snowpack's height is reduced by snow internal processes, such as water percolation, settling and compaction. During the second stage, the SWE decreases and meltwater production is modeled well using the energy balance model. Thus changes in snow height or simple temperature index models are not applicable for the prediction of runoff amounts and timing. At this site, melt

energies are predominantly supplied by radiation, which was also observed by *Harding and Lloyd* [1998] for the years 1995 and 1996.

[43] **Acknowledgments.** We gratefully acknowledge financial support by the Deutsche Forschungsgemeinschaft (Ro 1080/4-1&2), the European Union (LSF grant NP-98-5), and a research grant by the Deutsche Akademie der Naturforscher Leopoldina awarded to Julia Boike (BMBF-LPD 9901/8-11). Essential logistic support was provided by the German and the Norwegian Research Stations in Ny-Ålesund. Pier Paul Overduin was indispensable for the initial instrumentation of the site. Discussions were helpful with Annette Semadini-Davies, Larry Hinzman, Regine Hock, David Maréchal, Pier Paul Overduin and Kathy Young. Snow density data were collected by Knut Sand, David Maréchal and Oddbøjrn Bruland. Precipitation data from September 1998 to July 1999 were obtained from the Norwegian Meteorological Institute. Thanks to the anonymous reviewers who helped to improve the manuscript.

References

Boike, J., K. Roth, and P. P. Overduin, Thermal and hydrologic dynamics of the active layer at a continuous permafrost site (Taymyr Peninsula, Siberia), *Water Resour. Res.*, *34*, 355–363, 1998.

Braithwaite, R. J., Aerodynamic stability and turbulent sensible-heat flux over a melting ice surface, the Greenland ice sheet, *J. Glaciol.*, *41*, 562–572, 1995.

Brun, E., E. Martin, V. Simon, C. Gendre, and C. Coléou, An energy and mass model of snow cover suitable for operational avalanche forecasting, *J. Glaciol.*, *35*, 333–342, 1989.

Dingman, S. L., *Physical Hydrology*, 575 pp., Prentice-Hall, Old Tappan, N. J., 1994.

Førland, E. J., I. Hanssen-Bauer, and P. O. Nordli, Climate statistics and long term series of temperature and precipitation at Svalbard and Jan Mayen, *Rep. 21/97 KLIMA*, Norw. Meteorol. Inst., Oslo, 1997.

Gerland, S., J.-G. Winther, J. B. Ørbæk, G. E. Liston, N. A. Øritsland, A. Blanco, and B. Ivanov, Physical and optical properties of snow covering Arctic tundra on Svalbard, *Hydrol. Processes*, *13*, 2331–2343, 1999.

Harding, R. J., and C. R. Lloyd, Fluxes of energy and water from three high latitude tundra sites in Svalbard during the snowmelt and snow free periods, *Nord. Hydrol.*, *29*(4/5), 267–284, 1998.

Harstveit, K., Snowmelt modelling and energy exchange between the atmosphere and a melting snow cover, *Sci. Rep. 4*, 119 pp. Geophys. Inst., Univ. of Bergen, Norway, 1984.

Hinzman, L. D., D. L. Kane, and R. E. Gieck, Regional snow ablation in the Alaskan Arctic, in *Northern Hydrology: Selected Perspectives*, edited by T. D. Prowse and C. S. L. Ommaney, pp. 122–139, Nat. Hydrol. Res. Inst., Saskatoon, Sask., Canada, 1991.

Jordan, R., A one-dimensional temperature model for a snow cover: Technical documentation for SNTHERM89, *Spec. Rep. 91-16*, 49 pp., U.S. Army Cold Reg. Res. and Eng. Lab., Hanover, N.H., 1991.

Kane, D. L., R. E. Gieck, and L. E. Hinzman, Snowmelt modeling at small Alaskan Arctic watershed, *J. Hydrol. Eng.*, *2*, 204–210, 1997.

Liestøl, O., Pingos, springs, and permafrost in Spitsbergen, Årbok 1975, pp. 7–29, Norsk Polarinstit., Oslo, 1977.

Lundberg, A., Laboratory calibration of TDR-probes for snow wetness measurements, *Cold Reg. Sci. Technol.*, *25*, 197–205, 1997.

Marsh, P., and M. K. Woo, Wetting front advance and freezing of meltwater within a snow cover, 1, Observation in the Canadian Arctic, *Water Resour. Res.*, *20*, 1853–1864, 1984.

Price, A. J., and T. Dunne, Energy balance computations of snowmelt in a Subarctic area, *Water Resour. Res.*, *12*, 686–694, 1976.

Putkonen, J. K., Climatic control of the thermal regime of permafrost, northwest Spitsbergen, Ph.D. thesis, 121 pp., Univ. of Wash., Seattle, 1997.

Roth, K., and J. Boike, Quantifying the thermal dynamics of a permafrost site near Ny-Ålesund Svalbard, *Water Resour. Res.*, *37*, 2901–2914, 2001.

Sturm, M., J. P. McFadden, G. E. Liston, F. S. Chapin III, C. H. Racine, and J. Holmgren, Snow-shrub interactions in Arctic Tundra: A hypothesis with climatic implications, *J. Clim.*, *14*, 336–344, 2001.

Tarboton, D. G., D. G. Chowdhury, and T. H. Jackson, A spatially distributed energy balance snowmelt model, in *Biogeochemistry of Seasonally Snow-Covered Catchments, IAHS Publ. 228*, edited by K. A. Tonessen, M. W. Williams, and M. Tranter, pp. 141–155, Int. Assoc. Hydrol. Sci., Gentbrugge, Belgium, 1995.

Winther, J.-G., S. Gerland, J. B. Ørbæk, B. Ivanov, A. Blanco, and J. Boike, Spectral reflectance of melting snow in a high Arctic watershed on Svalbard: Some implications for optical satellite remote sensing studies, *Hydrol. Processes*, *13*, 2033–2049, 1999.

Woo, M. K., P. Marsh, and P. Steer, Basin water balance in a continuous permafrost environment, in *Proceedings of the Fourth International Conference on Permafrost*, pp. 1407–1411, Nat. Acad. Sci., Washington, D.C., 1983.

Woo, M. K., D. Yang, and K. L. Young, Representativeness of Arctic weather station data for the computation of snowmelt in a small area, *Hydrol. Processes*, *13*, 1859–1870, 1999.

Young, K. L., M. K. Woo, and S. A. Edlund, Influence of local topography, soil and vegetation on microclimate and hydrology at a high Arctic site, *Arct. Alp. Res.*, *29*, 270–284, 1997.

Zhang, T., T. E. Osterkamp, and K. Stamnes, Influence of the depth hoar layer of the seasonal snow cover on the ground thermal regime, *Water Resour. Res.*, *32*, 2075–2086, 1996.

Zhang, T., S. A. Bowling, and K. Stamnes, Impact of the atmosphere on surface radiative fluxes and snowmelt in the Arctic and Subarctic, *J. Geophys. Res.*, *102*, 4287–4302, 1997.

J. Boike, Water and Environmental Research Center, University of Alaska, Fairbanks, Fairbanks, AK 99775, USA. (ffjb2@aurora.uaf.edu)

O. Ippisch and K. Roth, Institute of Environmental Physics, University of Heidelberg, D-69120 Heidelberg, Germany. (kurt.roth@iup.uni-heidelberg.de; olaf.ippisch@iwr.uni-heidelberg.de)